Distributed Acoustic Sensing (DAS) of Seismic Properties in a Borehole drilled on a Fast-Flowing Greenlandic Outlet Glacier

Adam D Booth[1], Poul Christoffersen[2], Charlotte Schoonman[2], Andy Clarke[3], Bryn Hubbard[4], Rob Law[2], Samuel H Doyle[4], Tom R Chudley[2], Athena Chalari[3]

1. Institute of Applied Geoscience, School of Earth and Environment, University of Leeds, LS2 9JT, UK.

2. Scott Polar Research Institute, Department of Geography, University of Cambridge, Lensfield Road, Cambridge, CB2 1ER, UK.

3. Silixa Ltd, Silixa House, 230 Centennial Park, Centennial Avenue, Elstree, Wd6 3SN, UK

4. Centre for Glaciology, Department of Geography and Earth Sciences, Aberystwyth University, Aberystwyth, SY23 3DB, UK

Corresponding author: Adam Booth (a.d.booth@leeds.ac.uk)

Key Points:

- Distributed Acoustic Sensing (DAS) is a novel seismic surveying technology which uses fibre-optic cables to record seismic energy.
- We present the first glaciological application of DAS, installing cable in a 1030 m-long borehole drilled on Greenland's Store Glacier.
- We evidence, at 10 m vertical resolution, anisotropic and temperate ice beyond ~850 m depth and ~20 m of consolidated subglacial sediment.

Abstract

Distributed acoustic sensing (DAS) is a new technology in which seismic energy is recorded at high spatial and temporal resolution along a fibre-optic cable. We show analyses from the first glaciological borehole deployment of DAS to measure the englacial and subglacial seismic properties of Store Glacier, a fast-flowing outlet of the Greenland Ice Sheet. By characterizing compressional and shear wave propagation in 1030 m-deep vertical seismic profiles, sampled at 10 m vertical resolution, we detected a transition from isotropic to anisotropic ice consistent with a Holocene-Wisconsin transition at 83% of the ice thickness. We also infer temperate ice in the lowermost 100 m of the glacier, and identified subglacial reflections originating from the base of a 20 m-thick layer of consolidated sediment. Our findings highlight the transformative potential of DAS to inform the physical properties of glaciers and ice sheets.

Plain Language Summary

The seismic properties of glaciers and ice masses have a fundamental influence on ice flow, and help inform predictive models of how ice dynamics will evolve. Distributed acoustic sensing (DAS) is a revolutionary technology for seismic surveying, in which fibre-optic cables are used to record seismic waves with unprecendented resolution. Our paper presents data from the first glaciological deployment of a DAS system which we installed in a 1030 m-deep vertical borehole on Store Glacier, a fast-flowing outlet of the Greenland Ice Sheet. The detailed seismic anatomy of the glacier that our survey provides – an independent measurement of the seismic response every 10 m – gives new insights about its internal flow regime and temperature, and even allows us to detect layers of sediment underlying it. We predict that DAS surveying will play an increasingly large role in future glaciological seismic surveys as the recognition of its transformative potential grows.

1. Introduction

Seismic methods are widely applied in glaciology to quantify the englacial and basal properties of ice masses. Seismic velocity variations can indicate the strength and style of ice crystal fabrics (e.g., Diez et al., 2015; Smith et al., 2017; Brisbourne et al., 2019) and quantify intracrystalline water and debris (Hauck et al., 2011). Seismic attenuation rates vary with englacial temperature (Peters et al., 2012), and seismic reflectivity helps constrain the composition of subglacial material (e.g., Anandakrishnan, 2003; Dow et al., 2013). Combined estimates of compressional (P-) and shear (S-) wave velocities yield mechanical properties such as Poisson's ratio and bulk/shear moduli (e.g., Polom et al., 2013; Kulessa et al., 2019).

Most glaciological seismic acquisitions install receivers at, or close to, the glacier surface. Although logistically practical, quantitative interpretations of the resulting data make numerous assumptions about seismic propagation. Velocities derived from englacial or basal reflections typically make hyperbolic travel-time approximations, and estimates of physical properties (internal layering or e.g., bed reflectivity) must compensate for propagation processes between the source, the target and receivers. Although a paucity of ground-truth data can be mitigated using data-driven corrections (e.g., King et al., 2008; Peters et al., 2008, 2012), derivations of seismic quantities often remain under-constrained. The problem is exacerbated for passive seismic datasets, where source positions are unknown and location algorithms must assume background velocity/attenuation structures (e.g., Röösli et al., 2014; Podolskiy and Walter, 2016).

Borehole seismic deployments are advantageous because they (i) enable calibration of surface seismic responses and (ii) sample and provide local *in situ* seismic quantities. Data interpretation using a 'vertical seismic profile' (VSP) geometry invokes fewer travel-time assumptions than the surface seismic case, improving the accuracy of local seismic property estimates. These properties can extend to velocity and velocity anisotropy (Diez et al., 2015), attenuation (Beckwith et al., 2017) and reflection coefficient (Lira et al., 2012). Furthermore, VSP surveying offers a measurement of englacial seismic properties even for homogeneous ice columns that feature no internal reflectivity.

Seismic studies have benefited from the recent development of distributed acoustic sensing (DAS). DAS systems involve sending laser pulses into a fibre-optic cable from an *interrogator* unit. As they travel, a fraction of these pulses is backscattered via Rayleigh scattering, with the phase-lag in the backscattered pulse changing as the cable is strained, e.g., by the passage of seismic wavelets. Phase-lags are measured by the interrogator and used to simultaneously reconstruct the seismic response along the cable (Hartog et al., 2013). A length of fibre-optic cable therefore acts as a continuous geophone string. Besides their interpretative potential, DAS methods are logistically attractive in glaciology; e.g., conventional borehole seismic instruments may be lost in deforming/freezing boreholes, whereas DAS cables are designed to freeze in place even if they ultimately snap under englacial strain. As with conventional geophones, DAS systems can record in active and passive modes, enabling glacier seismicity to be monitored at high temporal and vertical resolution. DAS VSP datasets therefore offer powerful potential for *in situ* monitoring of englacial seismic properties.

Here, we interpret data from the first deployment of DAS technology within a glacier borehole. The survey was performed during the summer of 2019 on fast-flowing Store Glacier in West Greenland. We highlight the scope of the VSP DAS dataset, determining i) the vertical P-wave velocity and attenuation structure of the ice column, ii) Poisson's ratio using combined P- and S-wave arrivals, and ii) seismic properties and thickness of subglacial sediment layers.

2. Field setting and deployment

Store Glacier (Greenlandic: *Sermeq Kujalleq*) is a marine-terminating outlet glacier that drains ~34,000 km^2 of the Greenland Ice Sheet, and flows into Uummannaq Fjord (Rignot et al., 2008). Previously, the subglacial environment of the glacier was targeted at site S30 (inset, Figure 1) with boreholes drilled by pressurised hot water. Here, flow speeds of 600 m a^{-1} occur in response to high basal water pressure (Doyle et al., 2018) over a sedimentary bed (Hofstede et al., 2018).

In July 2019, boreholes were drilled in the centre of supraglacial lake site L028 (70.56793°N 50.08697°W; Figure 1), which drained via hydrofracture on 31 May 2019 (Chudley et al., 2019). A vertical borehole was instrumented with a Solifos BRUsens fibre-optic cable, installed to ~1030 m depth; the rapid loss of borehole water into a basal hydrological system confirms that the borehole, and therefore the cable, terminates at the glacier bed. The cable contained two single-mode fibres (for DAS) and four multi-mode fibres (for distributed temperature sensing, DTS, to be reported elsewhere), enclosed in a gel-filled stainless-steel capillary tube, with 4.8 mm-diameter polyamide sheathing and steel wire reinforcement. DAS VSPs were then recorded during a 3-day period, between 6-8 July 2019.

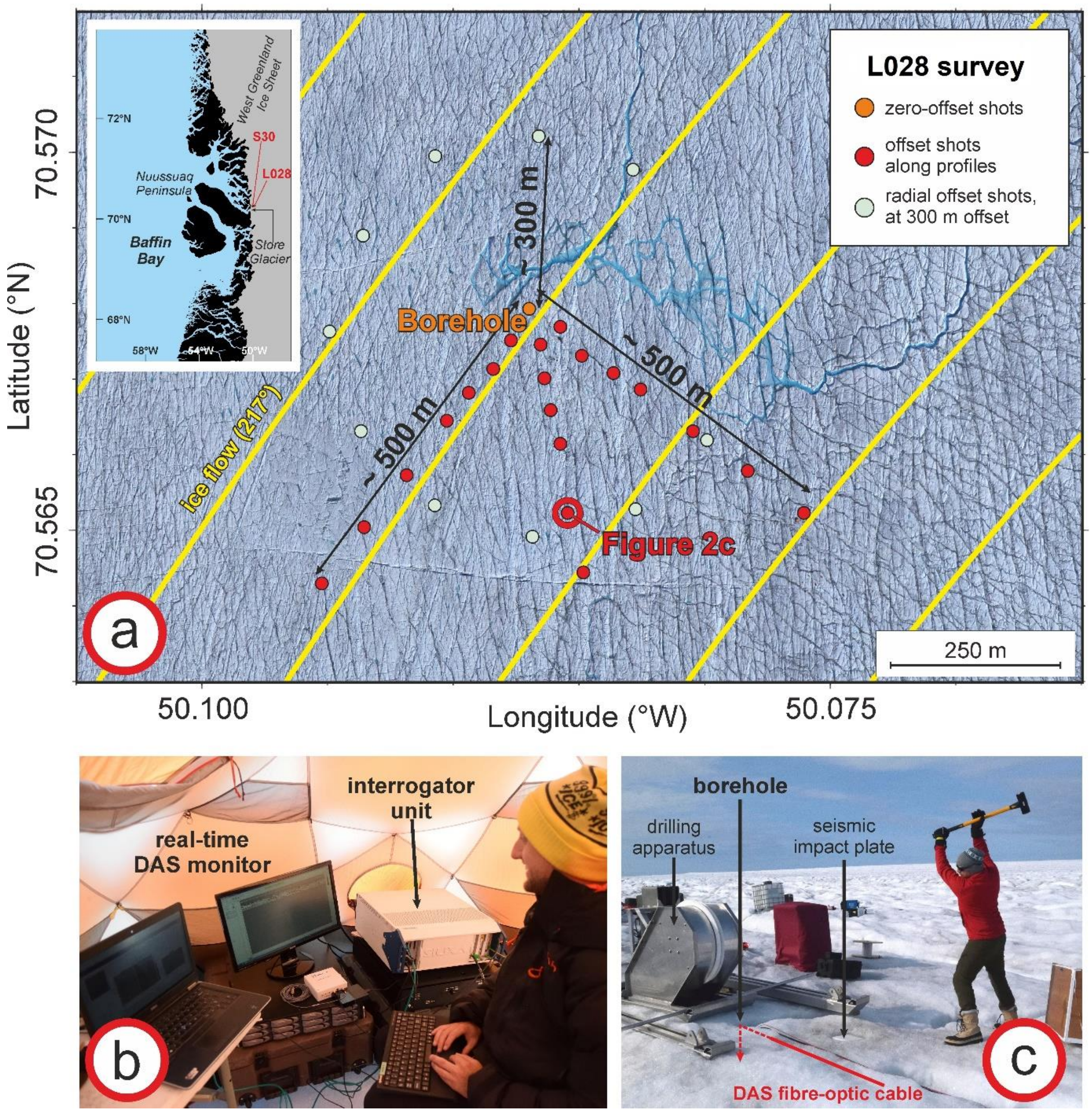

Figure 1. a) Location of seismic shots (red, grey) around the L028 borehole (orange); yellow lines denote ice flow. Inset: Sites S30 and L028 in West Greenland. b) Silixa iDAS^{TM} interrogator and acquisition monitor. c) Zero-offset VSP hammer shot.

A Silixa iDAS™ interrogator (Figure 1b), recording at 4000 Hz sampling frequency, established the seismic response every 1 m along the cable. However, the effective resolution of the acquisition is 10 m because the backscattered phase-lag is measured over a ~10 m 'gauge length'. Cable sensitivity varies as a function of the incidence angle, θ, of seismic energy to the cable axis, as $\cos^2\theta$ for P-waves and $\sin^2\theta$ for vertically-polarized shear (SV-) waves (Mateeva *et al.*, 2014). The system is insensitive to horizontally-polarized shear (SH-) waves. For the vertical installation reported here, the cable is most sensitive to vertically-propagating P-waves, and insensitive to those travelling horizontally. The converse holds for SV-waves.

Seismic energy was generated with a 7 kg sledgehammer striking a polyethylene impact plate (dimensions 0.20x0.20x0.05 m). Shots were made (i) ~1 m away from the borehole top (effectively zero-offset; Figure 1c), (ii) along azimuths parallel, orthogonal and at 45° to ice flow (~217°), up to 500 m offset from the borehole, and (iii) radially, at 30° intervals, at 300 m nominal offset from the borehole. For stacking, ~30 hammer strikes were recorded at each location over a ~4 minute period. Recorded seismic wavelets were consistent, and the typical correlation coefficient between successive traces in a shooting sequence is >0.96).

The fibre-optic cable was monitored in a passive mode. Zero-offset shots were extracted from the record by identifying the earliest arrival of seismic energy at the approximate time of shooting. For offset shooting, impact times were recorded with a GPS-synchronized surface geophone installed within 1 m of the impact place, and later used to extract data from the passive DAS record. These times are typically accurate to ±1 ms; residual static corrections, typically <±0.75 ms, were applied to synchronize shots prior to stacking.

3. VSP Data

Two VSPs are shown (Figure 2), acquired with zero-offset (2a,b) and offset (2c,d) geometries, on 7 July 2019 (12:15 and 20:00 UTC respectively). The source in the offset VSP is located 306.4 m south of the borehole (see Figure 1), hereafter termed '300 m offset'. Prominent arrivals are annotated for each record, together with initial velocity assessments. The enlarged panels in Figure 2b show direct-wave first-break picks for each trace (red crosses) and the mean and standard deviation of these within each 10 m gauge length (blue symbols). VSP acquisition geometries are described in the Supporting Information.

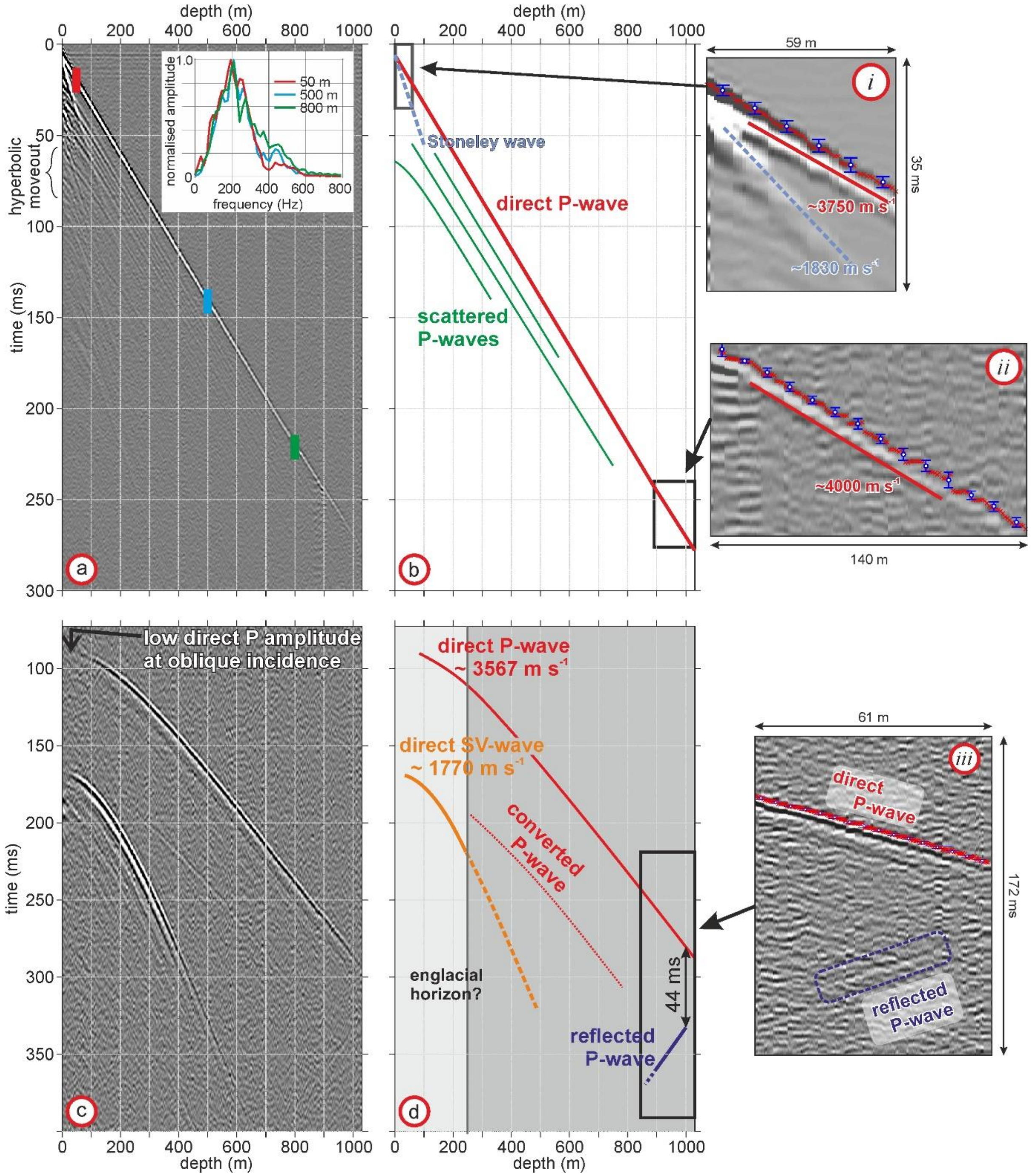

Figure 2. a) Zero-offset VSP; inset, amplitude spectra at 50 (red), 500 (blue) and 800 m (green) depths. b) Identification of arrivals in (a). c) 300 m offset VSP. d) Identification of arrivals in (c). Panels *i-iii* show enlarged sections of VSP data; red crosses show first-break picks, and blue symbols show their mean and standard deviation across a gauge length (blue).

3.1 Zero-offset VSP

The dominant arrival in the zero-offset record is the direct P-wave (Figure 2b), with linear moveout and no abrupt gradient changes, hence suggesting no strong englacial P-wave velocity (v_P) contrasts. However, linear trends fitted in shallow and deep intervals suggest a subtle v_P increase with depth: ~3750 m s^{-1} in the upper 50 m, versus ~4000 m s^{-1} in the lowermost 150 m (panels *i*, *ii*). The direct wave amplitude spectrum is stable throughout the VSP, with a dominant frequency of ~200 Hz and a bandwidth of ~200 Hz (inset, Figure 2a). The absence of a basal reflection at 1030 m depth is consistent with the low-reflectivity bed observed previously but, is consistent with low-reflectivity bed conditions observed previously (Hofstede et al., 2018).

Events that parallel the direct wave are interpreted as P-wave energy backscattered from, e.g. surface crevasses. In the upper 100 m of the VSP, between 50 and 70 ms, these arrivals have hyperbolic moveout, consistent with an origin offset from the borehole top. The linear arrival following the direct wave has a velocity of ~1830 m s^{-1}, close to the typical S-wave velocity (v_S) in ice. This arrival is interpreted as a Stoneley wave (Cheng and Toksöz, 1981), a vertically-travelling phase that propagates at a solid-solid interface, assumed to be the refrozen borehole wall.

3.2 300 m offset VSP

The offset VSP features a prominent hyperbolic direct P-wave (Figure 2c), detectable only below ~70 m given the near-perpendicular arrivals at such shallow depths. The best-fit hyperbola to the upper 200 m of direct P-wave travel-times gives v_P of 3567 ±7 m s^{-1} (Figure 2d). The later hyperbolic event (zero-depth arrival time ~160 ms) is the direct SV-wave and its best-fit hyperbola defines v_S of 1770 ±2 m s^{-1} for the upper 200 m. SV-wave amplitudes decay rapidly with depth due to combined propagation losses and cable sensitivity. Neither arrival shows an abrupt change in curvature, although a P-wave trend appears to diverge from the direct SV-wave from depths >250 m. This is interpreted as a SV-to-P mode conversion, and requires there to be a horizon around 250 m depth. This must represent a subtle change in P- and SV-wave velocities to suppress reflectivity but offers a strong velocity increase from SV- to P- propagation, given that compressional waves typically travel 2-times faster in ice than shear.

Consistent with the zero-offset VSP, there is no apparent P-wave basal reflection, but a low-amplitude reflection *is* still visible in the lowermost 150 m (panel *iii*). This event does not converge on the direct wave but, at the deepest point that it is visible (~990 m), lags it by ~44 ms. Since the borehole terminates at the glacier bed, at 1030 m, this reflection must originate subglacially, propagating through a velocity:thickness model that defines a ~44 ms two-way travel-time.

4. Quantitative VSP Interpretation

4.1 Vertical velocity model

Owing to the vertical cable and wave propagation, v_P in any depth interval is the depth difference between two observation points, divided by the travel-time of energy between them. We calculate travel-times by cross-correlating traces from different depth intervals and recording the time-lag of the cross-correlation peak. Thus, the velocity obtained is the average P-wave interval velocity within the correlation gap, with longer gaps increasing the degree of vertical smoothing.

Vertical v_P trends are estimated for correlation gaps of 20, 50 and 100 m (grey, red, blue, respectively, in Figure 3a). The 20 m gap offers high vertical resolution but is noisy since errors in identifying the cross-correlation lag (±1 digital sample, = 0.25 ms) are a greater proportion of the interval travel-time. Both 50 and 100 m trends show constant v_P of 3700 ±70 m s^{-1} in the upper 800 m, rising to 4100 ±70 m s^{-1} between 800 and 900 m depth, and decreasing to 3850 ±70 m s^{-1} in the lowermost 100 m. Curve widths represent the velocity uncertainty from misidentifying the peak cross-correlation lag by ±0.25 ms, but the trend is evident regardless of these errors or the correlation gap hence is considered as a genuine velocity feature.

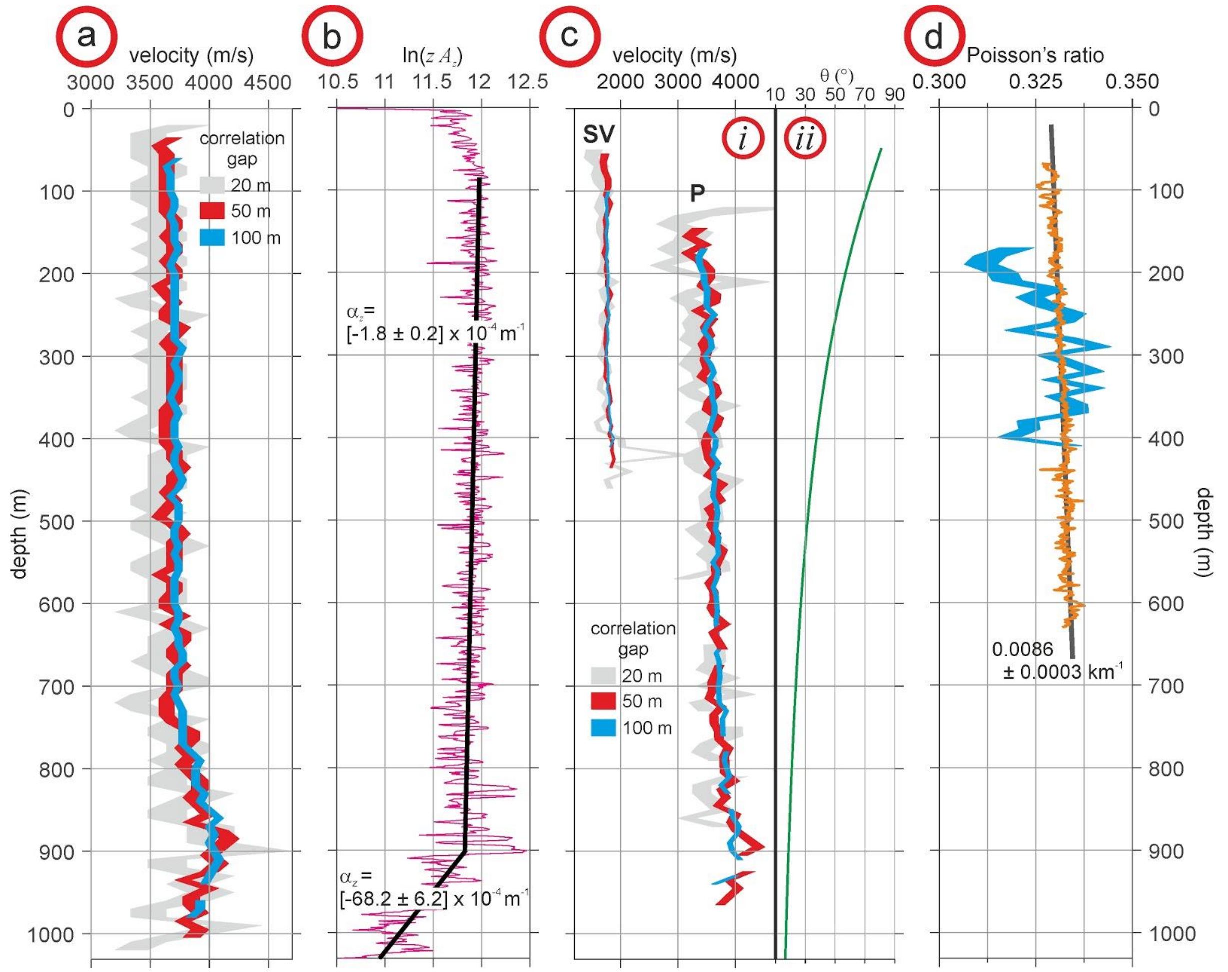

Figure 3. a) Depth variation of vertical v_P, estimated using VSP cross-correlation gaps of 20 m (grey), 50 m (red) and 100 m (blue). Curve width relates to ±0.25 ms error in identifying cross-correlation peaks. b) Amplitude decay attributable to anelastic attenuation. Black lines show best-fit linear trends in intervals 85 to 900 m, and 900 to 1030 m. c) As (a), but showing v_P and v_S derived from the 300 m offset VSP (i). Green trend in (*ii*) shows the incidence angle, θ, of direct waves to the cable axis. d) Local variation of Poisson's ratio (blue), and the raypath-averaged Poisson's ratio trend (orange).

4.2 Vertical attenuation model

The amplitude, A_x, of a seismic wave decreases with propagation due to geometric spreading and anelastic attenuation losses, expressed as:

$$A_x = A_0 G(x) e^{-\alpha x} \quad (1)$$

where A_0 is initial amplitude, $G(x)$ is geometric spreading losses, α is an attenuation coefficient and x is the distance travelled. For the zero-offset VSP, this distance is the depth, z, of the observation point along the fibre-optic cable, hence $G(x)$ varies as z^{-1}. Therefore, on rearranging Equation (1) as

$$\alpha_z = -z \ln\left(\frac{zA_z}{A_0}\right), \quad (2)$$

the gradient in a plot of z against $\ln\left(\frac{zA_z}{A_0}\right)$ defines the depth-averaged attenuation coefficient, α_z.

The P-wave attenuation coefficient is related, via v_P, to the seismic quality factor, Q, by

$$Q = \frac{-\pi f}{v_P \alpha_z}, \quad (3)$$

where f is wavelet frequency. Q has been related to englacial temperature (Peters et al., 2012), with warmer ice associated with lower-Q values and therefore increased attenuation. Peters et al. (2012) measure Q from englacial reflections using spectral ratios (Dasgupta and Clark, 1998). In our data, the consistency of spectra (Figure 2a) suggests that Q is high and spectral ratios could be influenced more by noise than genuine attenuation signatures. We therefore measure α_z, and therefore Q, from the amplitude decay of the direct P-wave.

Following corrections for spreading losses and assuming A_0 = 1, the depth variation of direct wave amplitudes (Figure 3b) has three linear sections. The increase of amplitude to ~85 m depth is non-physical and attributed to interference with the Stoneley wave. Between 85 and 900 m, amplitudes decay linearly and imply α_z of [-1.8 ±0.2] x 10^{-4} m^{-1}. For the lowest ~100 m, α_z is [-68.2 ±6.2] x 10^{-4} m^{-1}. Assuming the v_P derived previously and a dominant wavelet frequency of 200 Hz, Equation 3 implies Q_{200} of 925 ±120 and 24 ±3 respectively in these intervals.

4.3 Shear wave velocity and Poisson's ratio

Poisson's ratio describes how a material deforms when under stress, specifically the ratio of transverse extension to axial compression. In ice, Poisson's ratio is typically 0.3-0.34 (Köhler et al., 2019) but is sensitive to the strength of anisotropy (Nanthikesan and Shyam Sunder, 1994) and shows some tendency to increase with temperature (Weeks and Assur, 1967).

The dynamic Poisson's ratio, ν_d, is defined using v_P and v_S as:

$$\nu_d = \frac{\left(v_P/v_S\right)^2 - 2}{2\left[\left(v_P/v_S\right)^2 - 1\right]}\,. \qquad (4)$$

The variation of v_P and v_S (Figure 3c*i*) is measured from the offset VSP following the same cross-correlation procedure applied to the zero-offset data. However, since direct waves in the offset VSP arrive at an oblique angle θ to the cable axis (Figure 3c, inset *ii*), path length differences must be modified by the mean $\cos\theta$ within any given depth interval. These estimates neglect refraction effects (i.e., assume straight rays), but this is reasonable given the constant velocities observed through much of the ice column.

P-wave velocities are consistent with those in Figure 3a, including the velocity variation in the lowermost 200 m. An increase in v_P with depth is possible, potentially due to anisotropy or as an adverse consequence of assuming straight rays. Between 100-300 m, v_S is ~1740 ±20 m s^{-1}, and increases to ~1850 ±20 m s^{-1} at 450 m depth, albeit with the same straight-ray caveat.

Figure 3d shows two measures of Poisson's ratio. The first (orange curve) is path-averaged; under the straight-ray assumption, direct P- and SV-waves follow the same path, hence the ratio v_P/v_S is equivalent to the ratio of SV-to-P first-break travel-times. The mean Poisson's ratio recorded is 0.332 ±0.002, but this increases by 0.0086 ±0.0003 km^{-1} over the interval 80 to 620 m. The second measure is the discretized Poisson's ratio, estimated using v_P and v_S obtained for the 100 m correlation gap (thus limiting its evaluation to depths with mutual P and SV coverage). For this second case, Poisson's ratio increases to ~250 m depth, beyond which the mean value stabilizes at 0.331 ±0.007. Although the measurement of Poisson's ratio is smoothed over a 100 m interval, this depth is consistent with the apparent position of the mode-converting horizon apparent in Figure 2d, hence a transition in ice properties is inferred around this depth. In future analyses, the validity of these trends and the implied mode conversion will be explored using more sophisticated ray-tracing algorithms.

4.4 Thickness modelling of subglacial layering

Although the P-wave velocity and thickness of layering beneath the borehole cannot be determined uniquely, permissible v_P:thickness pairs satisfy a 44 ms two-way travel-time (Figure 2d). However, the deepest depth at which the reflection can reliably be perceived is 990 m, meaning 40 m of one-way propagation must be in basal ice. The travel-time contribution of the ice leg, t_{ice}, is

$$t_{ice} = \frac{2h}{v_{ice}\cos(i)} \quad (5)$$

where h is the distance above the glacier bed, v_{ice} is velocity through ice and i is the angle of incidence to the vertical (Figure 4a). For the offset VSP geometry, i is ~17° and v_{ice} is 3850 m s^{-1} (Figure 3). Therefore, Equation 5 shows that 22 ms of the 44 ms round-trip comprises propagation through ice, with the remaining 22 ms being travel-time through the subglacial layer, t_{sgl}. The thickness of this layer, h_{sgl}, is

$$h_{sgl} = \frac{1}{2} v_{sgl} t_{sgl} \cos(j), \quad (6)$$

where v_{sgl} is the subglacial layer velocity and j is the refracted angle into the subglacial layer (from Snell's law, $j = v_{sgl}\cos(i)/v_{ice}$). Equation 6 assumes a horizontal subglacial reflector, and negligible difference in incidence angles for the direct wave and the downgoing reflection leg (~0.6° for our geometry). The blue curve in Figure 4b shows pairs of v_{sgl} and h_{sgl} that satisfy t_{sgl} = 22 ms. Hofstede et al. (2018) gave v_P of 1839^{+1618}_{-94} m s^{-1} for subglacial material beneath site S30; assuming the same velocity at L028, h_{sgl} is 20^{+17}_{-2} m.

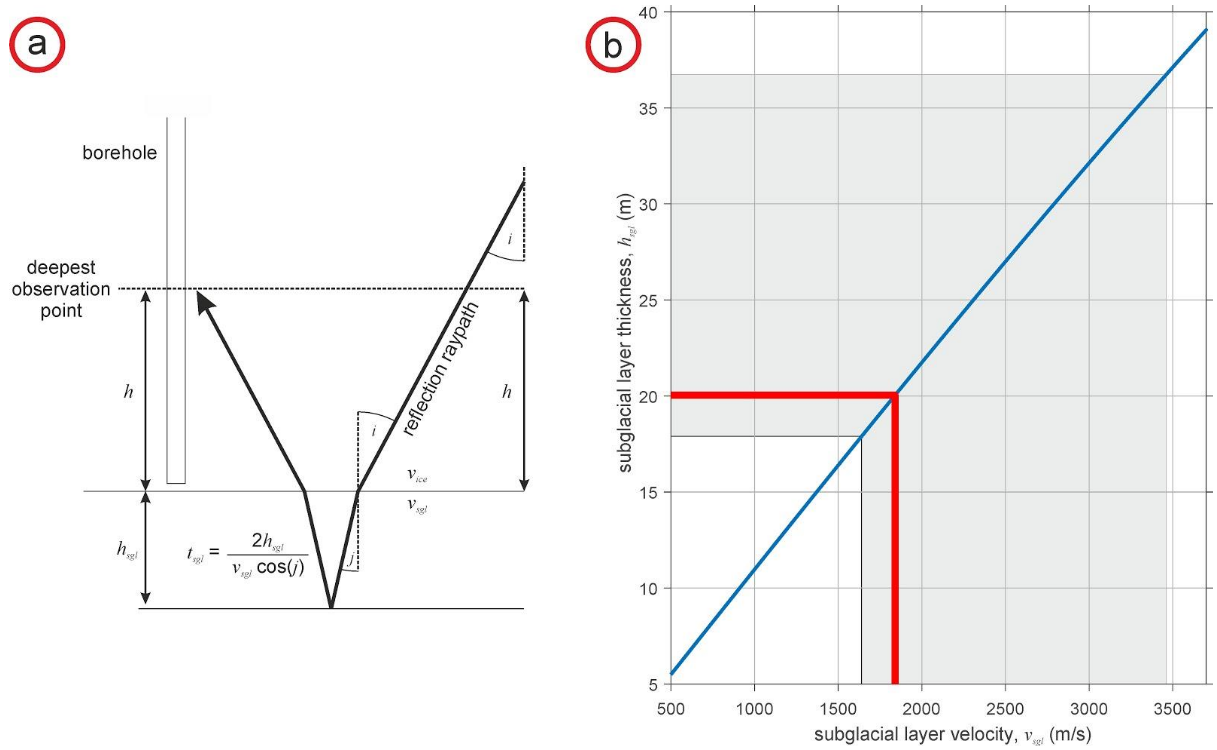

Figure 4. a) Schematic representation of Equations 5 and 6. b) Thickness estimation of subglacial layering, for v_{sgl}: h_{sgl} pairs that satisfy t_{sgl} = 22 ms. The grey shading shows the v_{sgl} range constrained for Store Glacier by Hofstede et al. (2018) and its corresponding h_{sgl}, with the red line showing h_{sgl} for their preferred velocity of 1839 m s^{-1}.

5. Discussion and conclusions

5.1 VSP analyses

The zero-offset VSP shows little v_P variation through the upper 800 m of Store Glacier, but increases to ~4100 ±70 m s^{-1} at ~850 m depth. This velocity is consistent with P-wave energy travelling vertically through anisotropic ice with a 0° cone opening angle (Diez et al., 2015). In our data, the transition to an anisotropic fabric appears gradational, attributable either to the vertical smoothing we apply or to a genuinely smooth transition that can only be detected given the finer vertical sampling provided by DAS recording. At site S30, Hofstede et al. (2018) detected an anisotropic transition in the lowermost ~80 m of Store Glacier, consistent with deformation recorded in the lowermost 100 m of the ice (Doyle et al., 2018), and interpreted it as the transition from Holocene- to Wisconsin-age ice (HWT). Our data suggest that the HWT beneath L028 is located at ~850 m depth, ~83% of ice thickness, matching reported estimates of 82-85% (Karlson et al., 2013).

Attenuation rates are low throughout most of the ice column, implying efficient propagation through cold ice, but increase by >2 orders of magnitude in the lowermost ~100 m. At these depths, we measure Q_{200} of 24 ±3, similar to values measured by Peters et al. (2012) for temperate ice (~-1 °C) at the base of Greenland's Jakobshavn Isbrae. We therefore predict similar conditions in the lowermost ice of Store Glacier. To what extent the v_P reduction in the lowermost 50 m of the ice column is related to temperate ice versus weaker anisotropy will be explored alongside co-located DTS records.

The offset VSP allowed constraint of both P- and SV- wave properties. Although englacial velocity contrasts were not detectable for either direct wave, a horizon appears to be present at ~250 m depth to convert SV- to P- wave energy. This may be associated with an increase in Poisson’s ratio, implying that the underlying ice is more deformable; again, DTS measurements will be used to investigate englacial temperatures at this depth.

Subglacial reflections were observed, originating beyond the borehole termination from the base of a layer that is 20^{+17}_{-2} m thick. Since the glacier bed has low reflectivity, the acoustic impedance of subglacial material must balance that of the basal ice (~3.5 x 10^6 kg m^{-2} s^{-1}). With v_{sgl} = 1839 m s^{-1}, the impedance contrast would be removed if the density of subglacial material was ~1900 kg m^{-3}. Considering the elastic properties tabulated in Christianson et al. (2014), this density implies that site L028 is underlain by consolidated, but neither deforming nor lithified, sediment.

5.2 DAS applicability

DAS methods are clearly beneficial for characterizing the seismic properties of ice masses at high resolution. Nonetheless, vertically-orientated fibre-optic cables are limited by their insensitivity to oblique particle motion; a well-coupled three-component geophone would record all senses of particle motion, including SH-waves that are undetectable with DAS. However, the ability of DAS to reconstruct independent seismic responses every ~10 m throughout the ice column can outweigh these shortcomings, particularly if the goal of the survey is to benchmark P-wave properties for conventional surface seismic analysis.

Our DAS cable has limited applicability as a horizontally-oriented receiver for surface-seismic surveying. Basal reflections would arrive with near-vertical incidence at the surface, hence with particle motion orthogonal to the cable axis. Considering Figures 2c and 3c*ii*, in which P-wave arrivals appear undetectable beyond ~70° incidence, reflections from a 1 km-deep target would only be detected at offsets >600 m. The recent development of *helically-wound* fibre-optic cables (Kuvshinov, 2015), sensitive to all directions of particle motion, could mitigate such limitations.

From a logistical perspective, once installed in a borehole, DAS recording is less challenging than, e.g., deploying downhole source or receiver tools. Such tools risk being frozen in place, hence must be used quickly and/or with compromised spatial sampling regimes.

5.3 Conclusions

We have demonstrated the feasibility and value of DAS surveying in glaciology. Our VSP acquisitions sample the seismic response, at 10 m vertical resolution, throughout the 1030 m thickness of a fast-flowing glacier in Greenland. These experiments allowed us to (i) measure the variation of P- and SV-wave properties, (ii) detect transitions relating to ice crystal fabric and temperature regimes in the lowermost 150 m of the glacier, and (iii) identify a subglacial layer of consolidated sediment up to 40 m thick. Extended analyses of these data will consider the azimuthal variation of the seismic response and the passive observations of natural seismicity around the L028 site, in conjunction with co-located pRES and DTS measurements.

We believe that DAS surveys will play an increasingly important role in glacier seismology, both in passive- and active-source modes, as the increasing recognition of the technique’s potential increases.

Acknowledgements

The authors declare no financial conflict of interest. This research was funded by the European Research Council as part of the RESPONDER project under the European Union's Horizon2020 research and innovation program (Grant 683043). BH was supported by a HERCW / Aberystwyth University Capital Equipment Grant. TRC and RL are supported by Natural Environment Research Council Doctoral Training Partnership studentships (grant NE/L002507/1). VSP stacking was performed by Diana Rosado (University of Leeds MSc Exploration Geophysics), and attenuation analyses benefitted from constructive discussions with Roger Clark.

Supporting data will be uploaded, following best practice, to a figshare repository. These will be the two VSP datasets presented in Figure 2.

References

Aki, K., & Richards, P.G. (2002), Quantitative Seismology, 2nd edition, University Science Books, Sausalito, California.

Anandakrishnan, S. (2003), Dilatant till near the onset of streaming flow of Ice Stream C, West Antarctica, determined by AVO (amplitude vs offset) analysis. *Annals of Glaciology*, *36*, 283-286. doi: 10.3189/172756403781816329.

Beckwith, J., Clark, R. & Hodgson, L. (2017), Estimating frequency-dependent attenuation quality factor values from prestack surface seismic data. *Geophysics, 82(1)*, O11-O22. doi: 10.1190/geo2016-0169.1

Brisbourne, A.M., Martín, C., Smith, A.M., Baird, A., Kendall, J.M. & Kingslake, J. (2019), Constraining recent ice flow history at Korff Ice Rise, West Antarctica, using radar and seismic measurements of ice fabric. *Journal of Geophysical Research: Earth Surface, 124(4851)*. doi: 10.1029/2018JF004776.

Cheng, C.H. & Toksöz, M.N. (1981), Elastic wave propagation in fluid-filled borehole and synthetic acoustic logs. *Geophysics, 46*, 1042-1053. doi: 10.1190/1.1441242.

Christianson, K., Peters, L.E., Alley, R.B., Anandakrishnan, S., Jacobel, R.W., Riverman, K.L., Muto, A. & Keisling, B.A. (2014), Dilatant till facilitates ice-stream flow in northeast Greenland. *Earth and Planetary Science Letters, 410*, 57-69. doi: 10.1016/j.espl.2104.05.060.

Chudley, T.R., Christoffersen, P., Doyle, S.H., Bougamont, M., Schoonman, C.M., Hubbard, B. & James, M.R. (2019), Supraglacial lake drainage at a fast-flowing Greenlandic outlet glacier, *Proceedings of the National Academy of Sciences, 116 (51),* 25468-25477. doi: 10.1073/pnas.1913685116.

Dasgupta, R. & Clark RA (1998), Estimation of *Q* from surface seismic reflection data, *Geophysics, 63(6),* 2120-2128. doi: 10.1190/1.1444505.

Diez, A., Eisen, O., Hofstede, C., Lambrecht, A., Mayer, C., Miller, H., Steinhage, D., Binder, T. & Weikusat, I. (2015), Seismic wave propagation in anisotropic ice - Part 2: Effects of crystal anisotropy in geophysical data, *The Cryosphere, 9,* 385-398. doi: 10.5194/tc-9-385.2015.

Dow, C.F., Hubbard, A., Booth, A.D., Doyle, S.H., Gusmeroli, A. & Kulessa, B. (2013), Seismic evidence of mechanically weak sediments underlying Russell Glacier, West Greenland, *Annals of Glaciology, 54(64),* 135-141. doi: 10.3189/2013AoG64A032.

Doyle, S.H., Hubbard, B., Christoffersen, P., Young, T.J., Hofstede, C., Bougamont, M., Box, J.E. & Hubbard, A. (2018), Physical conditions of fast glacier flow: 1. Measurements from boreholes drilled to the bed of Store Glacier, West Greenland, *Journal of Geophysical Research: Earth Surface, 123,* 324-348. doi: 10.1002/2017JF004529.

Hartog, A.H. (2017). An introduction to distributed optical fibre sensors. Boca Raton, Florida: CRC Press/Taylor and Francis.

Hauck, C., Böttcher, M. & Maurer, H. (2011), A new model for estimating subsurface ice content based on combined electrical and seismic data sets, *The Cryosphere, 5(2),* 453-468. doi: 10.5194/tc-5-453-2011.

Hofstede, C., Christoffersen, P., Hubbard, B., Doyle, S.H., Young, T.J., Diez, A., Eisen, O. & Hubbard, A. (2018), Physical conditions of fast glacier flow: 2. Variable extent of anisotropic ice and soft basal sediment from seismic reflection data acquired on Store Glacier, West Greenland, *Journal of Geophysical Research: Earth Surface*, *123*, 349-362. doi: 10.1002/2017JF004297.

Karlsson, N.B., Dahl-Jensen, D., Gogineni, S.P. & Paden, J.D. (2013), Tracing the depth of the Holocene ice in North Greenland from radio-echo sounding data, *Annals of Glaciology, 54*, 44-50. doi:10.3189/2013A0G64A057.

King, E.C., Smith, A.M., Murray, T. & Stuart, G. (2008), Glacier-bed characteristics of midtre Lovénbreen, Svalbard, from high-resolution seismic and radar surveying, *Journal of Glaciology, 54(184)*, 145-156. doi: 10.3189/002214308784409099.

Kulessa, B., Booth, A.D., O'Leary, M., King, E.C., Luckman, A.J., Holland, P.R., Jansen, D., Bevan, S.L., Thompson, S.S. & Hubbard, B. (2019), Seawater softening of suture zones inhibits fracture propagation in Antarctic ice shelves, *Nature Communications, 10, 5491*, 1-12. 10/1038/s41467-019-13539-x.

Kuvshinov, B.V. (2015), Interaction of helically wound fibre-optic cables with plane seismic waves, *Geophysical Prospecting, 64(3)*, 671-688. doi: 10.1111/1365-2478.12303.

Köhler, A., Maupin, V., Nuth, C. & van Pelt, W. (2019), Characterization of seasonal glacial seismicity from a single-station on-ice record at Holtedahlfonna, Svalbard, *Annals of Glaciology, 60(79)*, 23-36. doi: 10.1017/aog.2019.15.

Lira, J.E., Weglein, A.B., Bird, C.W. & Innanen, K.A. (2012), Determination of reflection coefficients by comparison of direct and reflected VSP events. *Journal of Seismic Exploration, 21(4)*, 361-376.

Mateeva, A., Lopez, J., Potters, H., Mestayer, J., Cox, B., Kiyashchenko, D., Wills, P., Grandi, S., Hornman, K., Kuvshinov, B., Berlang, W., Yang, Z. & Detomo, R. (2014). Distributed acoustic sensing for reservoir monitoring with vertical seismic profiling. Geophysical Prospecting, 62(4), 679-692. doi: 10.11111/1365-2478.12116.

Nanthikesan, S. & Shyam Sunder, S. (1994), Anisotropic elasticity of polycrystalline ice I_h. *Cold Regions Science and Technology, 22,* 149-169. doi: 10.1016/0165-232X(94)90026-4.

Peters, L.E., Anandakrishnan, S., Holland, C.W., Horgan, H.J., Blankenship, D.D. & Voigt, D.E. (2008). Seismic detection of a subglacial lake near the South Pole, Antarctica, *Geophysical Research Letters, 35,* L23501. doi: 10.1029/2008GL035704.

Peters LE, Anandakrishnan S, Alley RB and Voigt DE (2012). Seismic attenuation in glacier ice: a proxy for englacial temperature. Journal of Geophysical Research: Earth Surface. 117, F02008. 10.1029/2011JF002201.

Podolskiy, E.A. & Walter, F. (2016), Cryoseismology, *Reviews of Geophysics*, *54*, 7087-758. doi: 10.1002/2016RG000526.

Polom, U., Hofstede, C., Diez, A. & Eisen, O. (2014), First glacier-vibroseismic experiment – Results from cold firn of Colle Gnifetti, *Near Surface Geophysics, 12(4),* 493-504. doi: 10.3997/1873-0604.2013059.

Rignot, E., Box, J.E., Burgess, E., & Hanna, E. (2008), Mass balance of the Greenland ice sheet from 1958 to 2007, *Geophysical Research Letters, 35,* L20502. doi: 10.1029/2008GL035417

Röösli, C., Walter, F., Husen, S., Andrews, L.C., Lüthi, M.P., Catania, G.A. & Kissling, E. (2014), Sustained seismic tremors and icequakes detected in the ablation zone of the Greenland ice sheet, *Journal of Glaciology, 60(221),* 563–575. doi: 10.3189/2014JoG13J210.

Smith, E.C., Baird, A.F., Kendall, J.M., Martín, C., White, R.S., Brisbourne, A.M. & Smith, A.M. (2017), Ice fabric in an Antarctic ice stream interpreted from seismic anisotropy. *Geophysical Research Letters*, *44*, 3710-3718. doi: 10.1002/2016GL072093.

Weeks, W. & Assur, A. (1967), The Mechanical Properties of Sea Ice. US Army, Cold Regions Research and Engineering Laboratory, Monograph 11-C3.